Application of Optimal-Jerk Trajectory Planning in Gait Balance Training Robot

Yuan Fu
BUAA: Beihang University https://orcid.org/0000-0001-8082-4090
Dian-Sheng Chen (chends@buaa.edu.cn)
Beihang university and director of Robotics Institute
Xiao-Dong We
BUAA: Beihang University
Min Wang
BUAA: Beihang University

Original Article

Keywords: Gait and balance training robot, Balance training mode, Optimal trajectory planning

Posted Date: September 30th, 2020

DOI: https://doi.org/10.21203/rs.3.rs-82697/v1

Application of optimal-jerk trajectory planning in gait balance training robot

Fu Yuan, born in 1995, is currently a master candidate at Beihang. His research is mainly about rehabilitation training robot and motion control.
E-mail: yuanfu@buaa.edu.cn

Dian-Sheng Chen, professor of Beihang university and director of Robotics Institute. His research interests are fields of service robotics, bio-robotics, and intelligent mechatronics control technology. He has published over 70 articles in core journals and important international conferences, 50 of which are included by EI or SCI.
E-mail: chends@buaa.edu.cn

Xiao-Dong We, is currently a lecturer of Beihang university. He is engaged in robot mechanism design research.
E-mail: weixiaodong@buaa.edu.cn

Min Wang, is now associate professor of school of general engineering of Beihang university. She is committed to robot mechanism design.
E-mail: wmin@buaa.edu.cn；

Corresponding author：Dian-Sheng Chen E-mail：chends@buaa.edu.cn

Application of optimal-jerk trajectory planning in gait balance training robot

Fu Yuan[1] • Dian-Sheng Chen[1] • Xiao-Dong Wei[1] • Min Wang[1]

Abstract: Aiming at the gait and balance disorder of the elderly with the increase of age and the occurrence of various senile diseases, this paper proposes a novel gait balance training robot (G-Balance) based on a 6-DOF parallel platform. Based on the platform movement and IMU wearable sensors, two training modes, active and passive, have been developed to achieve vestibular stimulation. Virtual reality technology is also combined to achieve visual stimulation. In the active training mode, the elderly actively exercise to control the posture change of the platform and the switching of the virtual scene. In the passive training mode, the platform movement is combined with the virtual scene to simulate some bumpy environments such as earthquakes to enhance the human anti-interference ability. In order to achieve smooth switching of the scene, continuous speed and acceleration of the platform motion are required in some scenarios, in which trajectory planning algorithm is applied to meet the requirement. This paper expounds the application of trajectory planning algorithm in balance training mode.

Keywords: Gait and balance training robot • Balance training mode • Optimal trajectory planning

1. Introduction

As is known that vestibular sense and vision play an important role in the human balance system. Vestibular sense is responsible for perceiving changes in external acceleration and angular velocity, and visual sense perceives changes in the external environment[1]. Therefore, a type of gait balance training robot aims at combining motion platform to simulate acceleration and angular velocity changes with virtual reality technology to achieve visual simulation, thus to train human gait and balance capabilities. The representative of this type of robot is CAREN(Computer-Assisted Rehabilitation Environment) balance diagnosis and rehabilitation system (Motek, Amsterdam, The Netherlands)[2]. G-Balance also focuses on such problems. In some scenarios, in order to make the speed and acceleration of the motion platform change smoothly with the change of the virtual scene, trajectory planning is a splendid method to meet the requirement.

To achieve continuous changes in acceleration and velocity, commonly used trajectory equations are B-splines and cubic splines. In consideration of robot position, speed, acceleration constraints, the optimal trajectory planning is applied. The most prevailing optimality criteria are minimum execution time[3,4], minimum energy consumption[5,6] and minimum jerk[7,8]. The minimum energy consumption strategy and the minimum time strategy are generally used in energy consumption-sensitive or time-sensitive applications such as industry manipulators, which are not essential in our scenario. Therefore optimal-jerk planning is selected in G-Balance.

This paper explains in detail how the optimal-jerk is executed to make the movement of the robot goes smoothly with the change of virtual scene and how it is used in balance training mode.

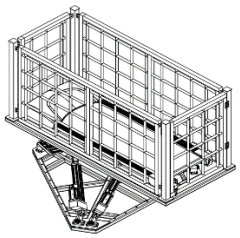

Figure 1 Structure of G-Balance

2. Structure and kinematics of the G-Balance system

The structure of G-Balance, as is shown in Figure 1, includes a classic 6-DOF parallel platform named stewart, a treadmill and safety guard like handrail and safety suspension mechanism(not shown in Figure 1). The platform is driven by 6 electric cylinders with power of 750W. Mecahnical schematic diagram of G-Balance is shown in Figure 2.

The mechanism can be divided into upper platform P and lower platform B. The upper and lower platforms are connected by universal hinges with hinge points naming P_i and B_i(i=1~6) respectively. The coordinate of the origin $\boldsymbol{P}$ of the upper platform relative to the lower platform is:

$$\boldsymbol{P} = \boldsymbol{P}_0 + \boldsymbol{T} = (x_0, y_0, z_0) + (x, y, z) \quad (1)$$

Where $\boldsymbol{P}_0$ is initial position vector and $\boldsymbol{T}$ is translation vector. Rotation adopts the representation of Euler angles. The corresponding rotation matrices are respectively shown below.

✉ Dian-Sheng Chen
chends@buaa.edu.cn
1 Robotics Institute, Mechanical Engineering and Automation Beihang University, Beijing 100191, China

$$\begin{cases} \boldsymbol{R}(\mathrm{z},\alpha) = \begin{bmatrix} cos\alpha & -sin\alpha & 0 \\ sin\alpha & cos\alpha & 0 \\ 0 & 0 & 1 \end{bmatrix} \\ \boldsymbol{R}(\mathrm{y},\beta) = \begin{bmatrix} cos\beta & 0 & sin\beta \\ 0 & 1 & 0 \\ -sin\beta & 0 & cos\beta \end{bmatrix} \\ \boldsymbol{R}(\mathrm{x},\gamma) = \begin{bmatrix} 1 & 0 & 0 \\ 0 & cos\gamma & -\sin\gamma \\ 0 & sin\gamma & cos\gamma \end{bmatrix} \\ \boldsymbol{R} = \boldsymbol{R}(\mathrm{z},\alpha)\cdot\boldsymbol{R}(\mathrm{y},\beta)\cdot\boldsymbol{R}(\mathrm{x},\gamma) \end{cases} \tag{2}$$

The position vector of the electric cylinder is expressed as:

$$\overrightarrow{B_iP_i} = \overrightarrow{BP} + \overrightarrow{PP_i} - \overrightarrow{BB_i} = \boldsymbol{T} + \boldsymbol{RP_i'} - \boldsymbol{B_i} = \boldsymbol{L_i} \tag{3}$$

Where $\boldsymbol{P_i'}$ indicates coordinate of upper hinge point relative to upper platform and $\boldsymbol{L_i}$ indicates the vector of the electric cylinder. So the length of the electric cylinder is:

$$L_i = \|\boldsymbol{L_i}\| = \sqrt{\boldsymbol{L_i^T L_i}} \tag{4}$$

The coordinate of the upper hinge point P_i and it's derivative is:

$$\boldsymbol{P_i} = \boldsymbol{RP_i'} + \boldsymbol{T} \tag{5}$$

$$\dot{\boldsymbol{P}}_{\boldsymbol{i}} = \dot{\boldsymbol{T}} + \boldsymbol{\omega} \times \boldsymbol{RP_i'} \tag{6}$$

The speed component of the upper hinge point in the direction of the electric cylinder is the speed of the electric cylinder.

$$\dot{L_i} = \left(\frac{\boldsymbol{L_i}}{L_i}\right)^{\boldsymbol{T}} \dot{\boldsymbol{P}}_{\boldsymbol{i}} \tag{7}$$

Similarly, the acceleration of the electric cylinder can be obtained, which we will not elaborate here since it is seldom used.

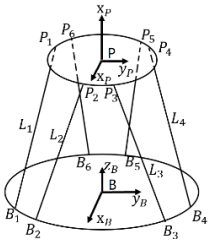

Figure 2 Mecahnical schematic diagram

3. Cubic splines for trajectory planning

Before we go further about the details, it's essential to illustrate the common symbols which are used in the latter derived formulas. These symbols and their concepts are shown in table 1.

In order to achieve continuous speed and acceleration, the most commonly used trajectory curve equations are cubic splines and quintic B-splines. Compared with the quintic B-splines, the cubic splines can not only perfectly satisfy the continuous speed and acceleration, but also avoid the oscillation and overshoot, which is why it was selected[7].

Table 1 Meaning of symbols

N	Number of electric cylinders (corresponding to hinge points)
$\boldsymbol{n}$	Maximum serial number of time point
$\boldsymbol{i}$	Serial number of time point, i= 0~n
$\boldsymbol{j}$	Serial number of electric cylinders, j = 1~N
$\boldsymbol{t_i}$	Discrete time point
$\boldsymbol{h_i}$	Time intervals, $h_i = t_{i+1} - t_i$
$\boldsymbol{q_{ji}}$	Space position coordinates of upper hinge point j corresponding to t_i
$\boldsymbol{M_{ji}}$	Acceleration of upper hinge point P_j at time t_i, $M_{ji} = Q_{ji}''(t_i)$
$\boldsymbol{VC_j}$	Maximum speed of electric cylinder j
$\boldsymbol{LC_j}$	Minimum speed of electric cylinder j
$\boldsymbol{AC_j}$	Maximum acceleration of electric cylinder j
$\boldsymbol{Q_{ji}(t)}$	Trajectory equation of upper hinge point P_j between time t_i and t_{i+1}

There are two main modes of trajectory planning for multi-joint robots: trajectory planning in the workspace and joint space. Trajectory planning in the working space is clearly visible and the end moves smoothly but may violate joint motion constraints or cause joint motion impact. Trajectory planning in the joint space, however, makes each joint move along the ideal trajectory, but the trajectory of the end of the mechanism cannot be displayed intuitively. Here we use joint space trajectory planning.

Given a series of time points and it's corresponding space position $(t_i, q_i)(i = 0,2,3 \ldots n-2, n)$ of the end, first we calculate the corresponding position of each upper hinge joint (t_i, q_{ji}) via inverse kinematics. Each segment of cubic splines satisfies the following relationship.

$$Q_{ji}(t) = a_{ji}(t-t_i)^3 + b_{ji}(t-t_i)^2 + c_{ji}(t-t_i) + d_{ji} \tag{8}$$

In order to obtain definite initial and ending speed and acceleration, here is a simple technique. Two virtual time points were inserted among (t_0, t_2), (t_{n-2}, t_n), which were indicated as $(\widetilde{t_1}, \widetilde{q_{j1}})$, $(\widetilde{t_{n-1}}, \widetilde{q_{j,n-1}})$. Gasparetto and Junsen Huang et al. adopted this technique[9,10]. Usually their values equal to:

$$\begin{cases} \widetilde{t_1} = \frac{t_0+t_2}{2} \\ \widetilde{t_{n-1}} = \frac{t_{n-2}+t_n}{2} \\ \widetilde{q_{j1}} = q_{j0} + h_0 v_0 + \frac{h_0^2}{3} a_0 + \frac{h_0^2}{6} \widetilde{M_1} \\ \widetilde{q_{j,n-1}} = q_{j,n} - h_{n-1} v_n + \frac{h_{n-1}^2}{3} a_n + \frac{h_{n-1}^2}{6} \widetilde{M_{n-1}} \end{cases} \tag{9}$$

Assume that the intial speed and acceleration is as follows.

$$\begin{cases} M_0 = a_0 \\ M_n = a_n \\ Q_{ji}'(t_0) = v_0 \\ Q_{ji}'(t_n) = v_n \end{cases} \tag{10}$$

At the same time, because of the continuous velocity and acceleration of the cubic splines, it is easy to derive the following formula.

$$\begin{cases} Q_{ji}(t_i) = q_{ji} \\ Q_{ji}(t_{i+1}) = Q_{j,i+1}(t_{i+1}) = q_{j,i+1} \\ Q'_{ji}(t_{i+1}) = Q'_{j,i+1}(t_{i+1}) \\ Q''_{ji}(t_{i+1}) = Q''_{j,i+1}(t_{i+1}) \end{cases} \quad (10)$$

Since $Q_{ji}(t)$ is a cubic function, its second derivative has a linear relationship with t. Perform linear interpolation on the acceleration.

$$Q''_{ji}(t) = \frac{t_{i+1}-t}{h_i} M_{ji} + \frac{t-t_i}{h_i} M_{j,i+1} \; t \in [t_i, t_{i+1}] \quad (11)$$

Due to the boundary condition $Q_{ji}(t_i) = q_{ji}, Q_{j,i+1}(t_{i+1}) = q_{j,i+1}$, we can obtain the following equations by integrating equation (10).

$$\begin{cases} Q_{ji}(t) = \frac{M_i}{6h_i}(t_{i+1}-t)^3 + \frac{M_{i+1}}{6h_i}(t-t_i)^3 + \\ \left(\frac{q_{ji}}{h_i} - \frac{h_i M_i}{6}\right)(t_{i+1}-t) + \left(\frac{q_{j,i+1}}{h_i} - \frac{h_i M_{i+1}}{6}\right)(t-t_i) \\ Q'_{ji}(t) = -\frac{M_i}{2h_i}(t_{i+1}-t)^2 + \frac{M_{i+1}}{2h_i}(t-t_i)^2 + \\ \frac{q_{j,i+1}-q_{ji}}{h_i} + \frac{M_i - M_{i+1}}{6} h_i \end{cases} \quad (12)$$

Because of the continuous speed, we can get the following equation from quation (12).

$$\frac{h_{i-1}}{h_{i-1}+h_i} M_{i-1} + 2M_i + \frac{h_i}{h_{i-1}+h_i} M_{i+1} = \frac{6}{h_{i-1}+h_i}\left(\frac{q_{j,i+1}-q_{ji}}{h_i} - \frac{q_{ji}-q_{j,i-1}}{h_{i-1}}\right) \quad (13)$$

Rewrite the above formula in matrix form:

$$\begin{cases} KM_j = B_j \\ M_j = [M_{j0}, M_{j1} \dots M_{jn}]^T \end{cases} \quad (14)$$

Finally, we get the complete cubic spline trajectory constraint equation.

4. Optimization of trajectory

Through cubic splines trajectory planning, the position, velocity and acceleration of the joint space are continuous, which basically meets the requirements. The mechanism is also subject to some other constraints resulting from motor performance and structural limitations. The most common ones are speed constraints and acceleration constraints, which is why minimum jerk trajectory planning is introduced.

The optimal trajectory planning is essentially a nonlinear equation optimization problem, the core of which is to find the constraint equation and the objective optimization equation. In the previous chapter, we have obtained the equality constraint. The objective optimization equation is to obtain the optimal jerk.

$$min: \sum_{j=1}^{6} \sum_{i=1}^{n-1} \frac{(\ddot{q}_{j,i+1} - \ddot{q}_{ji})^2}{t_{i+1}-t_i} \quad (15)$$

Meanwhile, the speed and acceleration constraint must be satisfied.

$$\begin{cases} |\dot{q}_j(t)| \le VC_j \\ |\ddot{q}_j(t)| \le AC_j \end{cases} \quad (16)$$

The velocity and acceleration constraint equations are infinite state equations, which are not easy to solve. According to Ref [9], some optimizations can be achieved. The velocity of any joint is a quadratic function, and its extreme value can only appear at the endpoint or the point where the acceleration is zero. The moment when acceleration of each segment is zero is as follows.

$$t^*_{ji} = t_i + \frac{h_i M_i}{M_i - M_{i+1}} \quad (17)$$

Therefore, the maximum speed of each segment can only be one of the following three:

$$\begin{cases} \dot{q}_j(t_i) = -\frac{M_i}{2} h_i + \frac{q_{j,i+1}-q_{ji}}{h_i} + \frac{h_i}{6}(M_i - M_{i+1}) \\ \dot{q}_j(t_{i+1}) = \frac{M_{i+1}}{2} h_i + \frac{q_{j,i+1}-q_{ji}}{h_i} + \frac{h_i}{6}(M_i - M_{i+1}) \\ \dot{q}^*_{ji} = -\frac{h_i}{2(M_{i+1}-M_i)} M_{i+1} M_i + \frac{q_{j,i+1}-q_{ji}}{h_i} - \frac{h_i}{6}(M_{i+1}-M_i) \\ \max\left(|\dot{q}_j(t_i)|, |\dot{q}_j(t_{i+1})|, |\dot{q}^*_{ji}|\right) \le VC_j \end{cases} \quad (18)$$

Similarly, acceleration is a linear function, so only the accelerations at the two ends need to meet the constraint conditions.

$$\max(|M_i|, |M_{i+1}|) < AC_j \quad (19)$$

Through the above analysis, the optimal-jerk trajectory planning is transformed into a nonlinear programming problem that satisfies equality constraints and inequality constraints which can be solved by sequential quadratic programming(SQP).

However, from the above derivation, it is easy to reach the conclusion that the time interval obtained by this method will be infinitely long. We can take advantage of the method in paper [9] to add a scale factor between the minimum time and the minimum jerk as following.

$$min: \alpha \sum_{i=0}^{n-1} h_i + \beta \sum_{j=1}^{6} \sum_{i=1}^{n-1} \frac{(\ddot{q}_{j,i+1} - \ddot{q}_{ji})^2}{t_{i+1}-t_i} \quad (20)$$

Another alternative is that we set a lower limit for the speed which we adopted here.

$$|\dot{q}_j(t)| \ge LC_j \quad (21)$$

The lower speed limit is determined by the longest running time we decided which is not the actual minimum speed along the way cause the speed in the beginning or at the end is zero in most cases. With this method, we can easily control the maximum time of each running. Similarly, we can set an equality constraint on time shown in equation (22)[11].

$$\sum h_i = T \quad (22)$$

It is worth noting that the time T set here cannot be less than the shortest running time,which is calculated by the following equation.

$$T_{min} = \max_j \left(\frac{\sum_{i=1}^{n-1} \text{abs}(q_{j,i+1} - q_{j,i})}{VC_j}\right) \quad (23)$$

It is difficult to identify which of the above methods is the best choice. Application scenarios are the most important consideration in choosing.

Making a brief summarization, the whole procedure of optimal-jerk planning is as follows:

(1) Given a series of points int the workspace, the position of corresponding upper hinge points were obtained through the inverse kinematics solution.

(2) According to the characteristics of the cubic spline, the equation constraint of the entire trajectory is obtained.

(3) According to the speed, acceleration, and time constraints, get the inequality constraints of the trajectory.

(4) Solve the nonlinear optimization problems by SQP or some other optimization methods.

5. Active and passive training mode

The core training function of G-Balance is to use the characteristics of the multi-degree-of-freedom motion platform to offer vestibular acceleration and angular velocity stimulation. At the same time, combined with virtual reality technology, visual stimulation and an immersive training experience can be achieved. Two training modes are proposed based on the system.

In the active training mode, the elder can exert influence and control strategy on the platform. In other words, this is similar to a somatosensory game with actual physical stimulation. To capture the posture of human, seven IMU inertial sensors are bound to the human instep, lower limbs, upper limbs and waist to capture the motion information of the human ankle, knee, and hip joints. The periodicity, symmetry, gait frequency and some other gait information are closely related to the movement of these joints which are essential to realize human gait assessment and simple gait training with treadmill[12-14]. Meanwhile, the output of these sensors is extracted and processed as the input of the robot control system, so as to realize the active control.

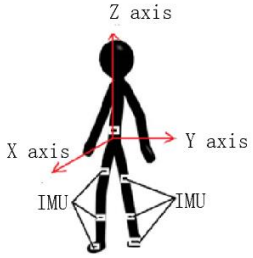

Figure 3 Position of the bounded sensors

The flow of control signals and one virtual training scene are shown in Figure 4 and Figure 5 respectively. This scene is similar to a surfing game. The movement of the lower limbs of the human body corresponds to the change of the posture of the virtual person, and the posture of the platform corresponds to the posture of the surfboard. All control information comes from the position changes of human body. We can simplify the human body into a skeleton model, which is composed of thighs, calves, trunk and so on thus the position of each joint can be obtained by the angle of each joint and the length of the limb.

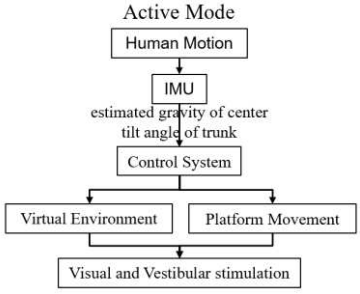

Figure 4 Flow of control signals in active mode

Figure 5 Virtual training scene

Once position of each joint is obtained which we donated as G_i here, we can roughly estimate the center of gravity of each limb. According to the research of Vanhan C L et al[16], There is a fixed proportional relationship between the center of gravity of each leg and the position of adjacent joints, which is shown in Figure 6 and equation (24).

$$\begin{cases} G_{Thigh,CG} = G_{Hip} + 0.39(G_{Knee} - G_{Hip}) \\ G_{Calf,CG} = G_{Knee} + 0.42(G_{Ankle} - G_{Knee}) \end{cases} \quad (24)$$

Here we use the weighted sum of the center of gravity of each limb and the angle of trunk tilt as the input signal of the control system, which is the position and euler angle of the working space. In other words, the position q_i here is the estimated center of gravity of human body.

$$q_i = \sum_{i=1}^{4} \mu_i G_i \quad (25)$$

Where G_i is the center of gravity of each lower limb and μ_i is the corresbonding weight. The next task is to use the trajectory planning method described in chapter 4 to execute trajectory planning. The sampling time interval of position q_i is very short, usually the frequency is 20 to 50 Hz. Therefore, we sample the position q_i at one-second intervals as the final input position in the working spaces.

In the passive traning mode, the platform combines with virtual environment to simulate some vibration scenes, training people's anti-interference ability. This training mode is similar to the earthquake hut in the science museum. In this scenario, the sensors are used to collect the response of the human body to stimuli. The trajectory of estimated center of gravity of human body is used to measure a person's balance

ability and training effect like the usage of center of pressure(COP)[17,18]. Unlike the two-dimensional COP method, the estimated center of gravity here is three-dimensional. The flow of signals in this mode is shown in Figure 7.

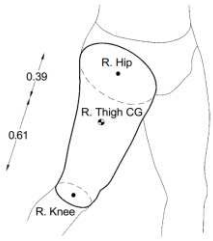

Figure 6 Location of the center of gravity corresponding to adjacent joints

In order to achieve more realistic acceleration and angular velocity stimulation in limited motion space, washout algorithm is introduced. Here we adopt the improved washout algorithm[19] to achieve better vestibular stimulation which will not go further elaboration.

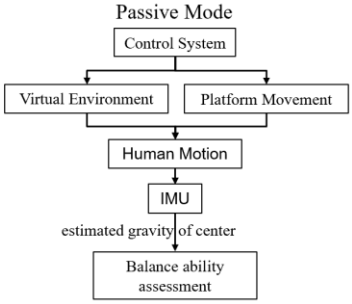

Figure 7 Flow of signals in passive mode

6. Simulation Results

Following the steps described above, given a series of positions in the working space, the corresponding joint space positions are calculated, as shown in Table 2 and Table 3 respectively. The kinematic limits of the electric cylinders are set the same cause the models are exactly identical.

As a comparison, we set the running time to 8s, and carry out the trajectory planning of the optimal-jerk and the ordinary cubic splines respectively. In the ordinary trajectory planning, we set via points at equal intervals, which is 1.6s in this case.

Table 2 Via points int the working space

Via points	Representation and unit $(x, y, z, \alpha, \beta, \gamma)$ (mm/deg)
1	(0,0,0,0,0,0)
2	(15,20,15,4,5,12)
3	(25,31,42,7,8,6)
4	(40,60,30,15,14,13)
5	(50,40,40,8,12,16)
6	(25,67,20,16,15,14)

Table 3 Via points in the joint space

Joint	Via points(mm)					
	1	2	3	4	5	6
1	657	657	657	657	657	657
2	712	634	725	657	715	585
3	702	685	729	716	701	601
4	724	682	760	727	711	527
5	722	660	779	711	754	541
6	733	665	755	722	699	524

Table 4 kinematic limits

Name	Velocity(mm/s)	Acceleration($\mathbf{mm/s^2}$)
Value	200	200

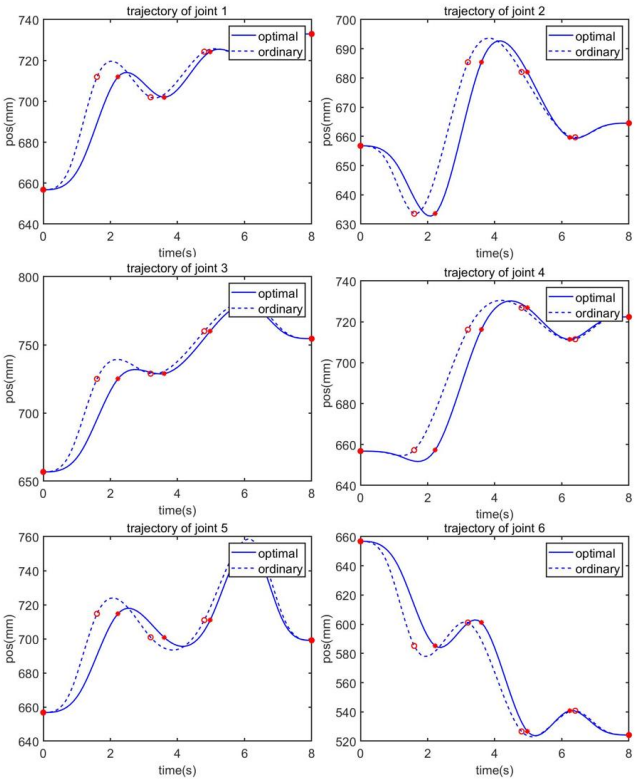

Figure 8 Trajectory of joints

The results of simulations are reported in Figures. 8-11, showing the position, velocity, acceleration of each joint and the total jerk respectively.

It can be seen from the simulation results that the trajectory, velocity, and acceleration are all continuous functions in the whole process. The running velocity and acceleration are within the limits. All the results are consistent with our theoretical derivation.

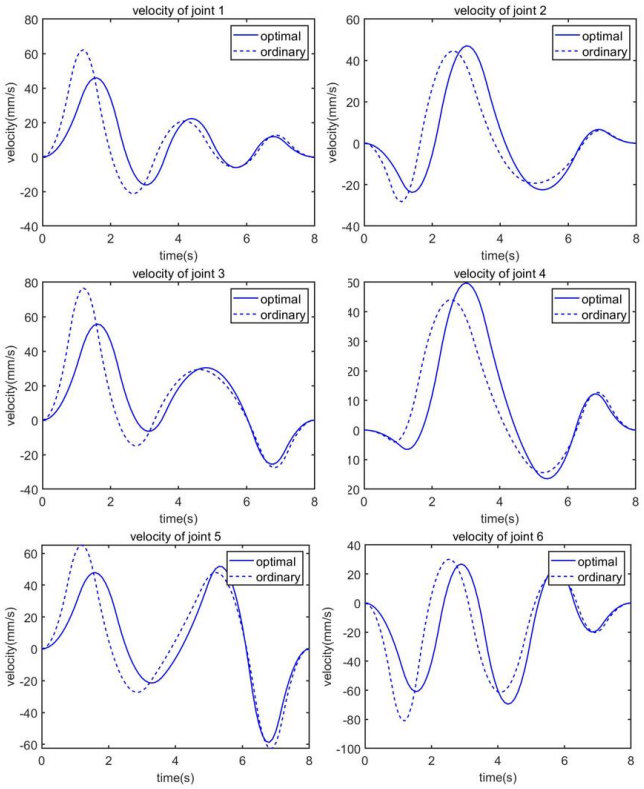

Figure 9 Velocity of joints

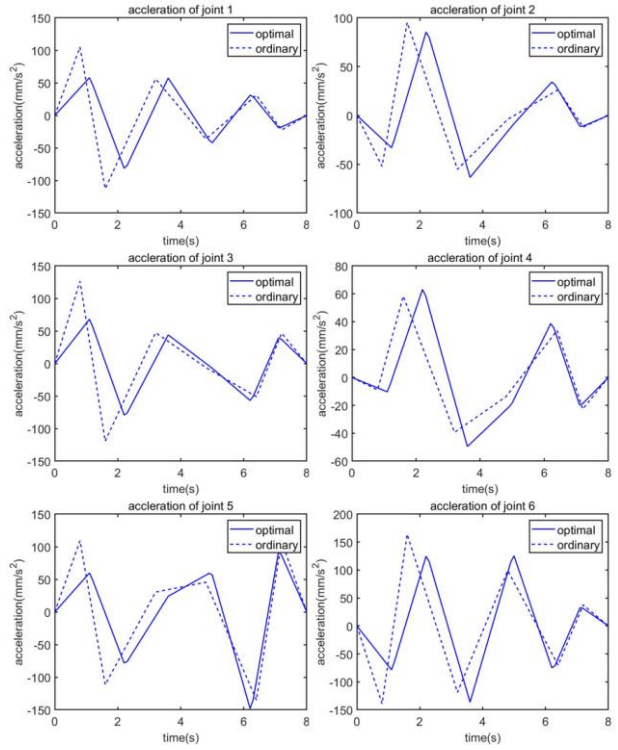

Figure 10 Acceleration of joints

The value of jerk obtained by the minimum jerk trajectory planning is 4.89×10^5 , which is 7.52×10^5 in the ordinary trajectory planning .The difference between the two is not much. Moreover, the speed and acceleration of the entire process are also within the range of kinematic limits in ordinary trajectory planning despite the fact that constraints are not included. The main reason for this result is that the platform's stroke is small, which leads to the similarity of the planned trajectories, making the minimum jerk method has no obvious advantage. As the distance between the position points in the workspace increases, the minimum jerk trajectory planning will gradually show advantages. The optimal-jerk trajectory planning, however, is still worth adopting considering the position, speed and acceleration constraints. It is worth noting that all via points in the workspace cannot exceed the stroke limit of the robot.

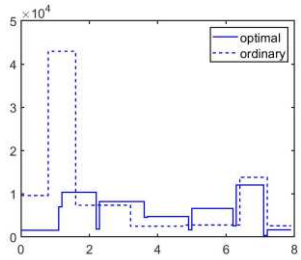

Fig 11 Jerk of joints

7. Conclusion

In some scenarios, G-Balance is required to move smoothly while satisfying the speed and acceleration constraints, so the optimal-jerk trajectory planning is introduced. In this article, detailed process of optimal-jerk trajectory planning is elaborated and its application in active training mode using the human movement as input signals is described. There are several key points to note.

(1) Cubic splines trajectory planning with virtual points added at the beginning and end makes the speed and acceleration of the starting and ending points controllable.

(2) In the optimal-jerk trajectory planning, there are three common methods to control time: add the time with weight to the objective function, add the minimum running speed limit and specify the running time. Which method to choose depends on the specific scenario.

(3) Due to the characteristics of cubic splines, continuous speed and acceleration constraints can be transformed into discrete constraints in a finite state, greatly simplifying the calculation process.

In the virtual scene listed in this article, the usefulness of trajectory planning is not obvious cause more virtual training scenarios are being designed. Meanwhile, the entire control system like washout algorithm and training mode like passive training mode of G-Balance are not described in detail.

Funding

Supported by National Key R&D Program of China（2018YFB1307002）

Availability of data and materials

The datasets supporting the conclusions of this article are included within the article.

Authors' contributions

The author' contributions are as follows: Fu Yuan was in charge of the whole algorithm implementation, coding and manuscript writing; Dian-Sheng Chen was responsible for the algorithm design and mathematical guidance; Xiao-Dong Wei assisted with balance training mode design; Min Wang revised the manuscript and made some improvements.

Competing interests

The authors declare no competing financial interests.

Consent for publication

Not applicable

Ethics approval and consent to participate

Not applicable

References

[1] Wolfe, Jeremy; Kluender, Keith; Levi, Dennis (2012). Sensation & perception (3rd ed.). Sinauer Associates. p. 7.

[2] CAREN balance rehabilitation training system official webpage. https://www.motekmedical.com/solution/caren/. Accessed 15 June 2017.

[3] Bobrow J E , Dubowsky S , Gibson J S . Time-Optimal Control of Robotic Manipulators Along Specified Paths[J]. Int. J. of Robotic Research, 1985, 4(3):3-17.

[4] Aurelio Piazzi, Antonio Visioli. Visioli, A.: Global minimum-time trajectory planning of mechanical manipulators using interval analysis. Int. J. Contr. 71(4), 631-652[J]. International Journal of Control, 2010, 71(4):631-652.

[5] Field G , Stepanenko Y . Iterative dynamic programming: an approach to minimum energy trajectory planning for robotic manipulators[C]. IEEE International Conference on Robotics & Automation. IEEE Xplore, 1996.

[6] Hirakawa A R , Kawamura A . Trajectory planning of redundant manipulators for minimum energy consumption without matrix inversion[C]. IEEE International Conference on Robotics & Automation. IEEE, 2002.

[7] Kyriakopoulos K J , Saridis G N , De Figueiredo R J P , et al. Minimum jerk trajectory planning for robotic manipulators[J]. 1991, 1387:159-164.

[8] Piazzi A , Visioli A . An interval algorithm for minimum-jerk trajectory planning of robot manipulators[C]. IEEE Conference on Decision & Control. IEEE, 1997.

[9] Gasparetto A , Zanotto V . A technique for time-jerk optimal planning of robot trajectories[J]. Mech.mach.theory, 2008, 24(3):415-426.

[10] Gasparetto A , Zanotto V . A new method for smooth trajectory planning of robot manipulators[J]. Mechanism & Machine Theory, 2007, 42(4):455-471.

[11] Piazzi A , Visioli A . Global minimum-jerk trajectory planning of robot manipulators[J]. IEEE Transactions on Industrial Electronics, 2000, 47(1):140-149.

[12] Moe-Nilssen R , Helbostad J L . Estimation of gait cycle characteristics by trunk accelerometry[J]. Journal of Biomechanics, 2004, 37(1):121-126.

[13] Piriyakulkit S , Hirata Y , Ozawa H . Real-time gait event recognition for wearable assistive device using an IMU on thigh[C]// 2017:314-318.

[14] Yun X , Calusdian J , Bachmann E R , et al. Estimation of Human Foot Motion During Normal Walking Using Inertial and Magnetic Sensor Measurements[J]. IEEE Transactions on Instrumentation & Measurement, 2012, 61(7):2059-2072.

[15] Tisserand R, T Robert,et al. A simplified marker set to define the center of mass for stability analysis in dynamic situations [J]. Gait & Posture,2016,48:64-67.

[16] Vanhan C L, Davis B L, Jeremy C O. Dynamics of human gait [M]. Cape town, South Africa: Kiboho Publishers,1992.

[17] GOTO,Masahiro, KUMADA,Hitoshi. The assessments of body sway on the static standing using the center of pressure[J]. Aino Journal, 2008, 7:21-26.

[18] Chu H H , Dong Z , Hans C , et al. Using dynamic center of pressure to measure human body's balance ability[C]. Gerontechnology. 2014.

[19] Asadi H , Mohamed S , Nahavandi S . Incorporating Human Perception With the Motion Washout Filter Using Fuzzy Logic Control[J]. IEEE/ASME Transactions on Mechatronics, 2015, 20(6):3276-3284.

Biographical notes

Fu Yuan, born in 1995, is currently a master candidate at Beihang. His research is mainly about rehabilitation training robot and motion control.
E-mail: yuanfu@buaa.edu.cn

Dian-Sheng Chen, professor of Beihang university. His research interests are fields of service robotics, bio-robotics, and intelligent mechatronics control technology. He has published over 70 articles in core journals and important international conferences, 50 of which are included by EI or SCI.
E-mail: chends@buaa.edu.cn

Xiao-Dong Wei, is currently a lecturer of Beihang university. He is engaged in robot mechanism design research.
E-mail: weixiaodong@buaa.edu.cn

Min Wang, is now associate professor of school of general engineering of Beihang university. She is committed to robot mechanism design.
E-mail: wmin@buaa.edu.cn

Figures

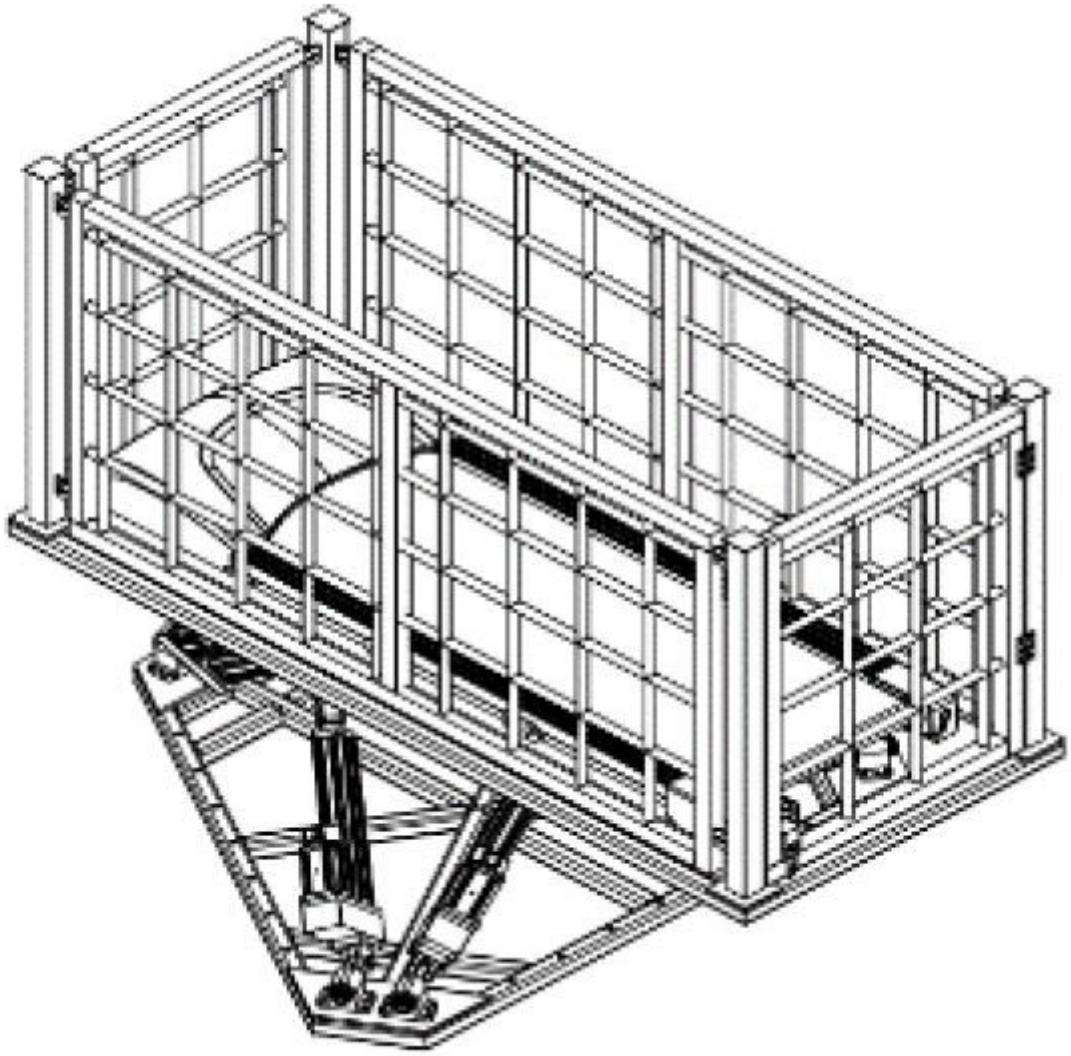

Figure 1

Structure of G-Balance

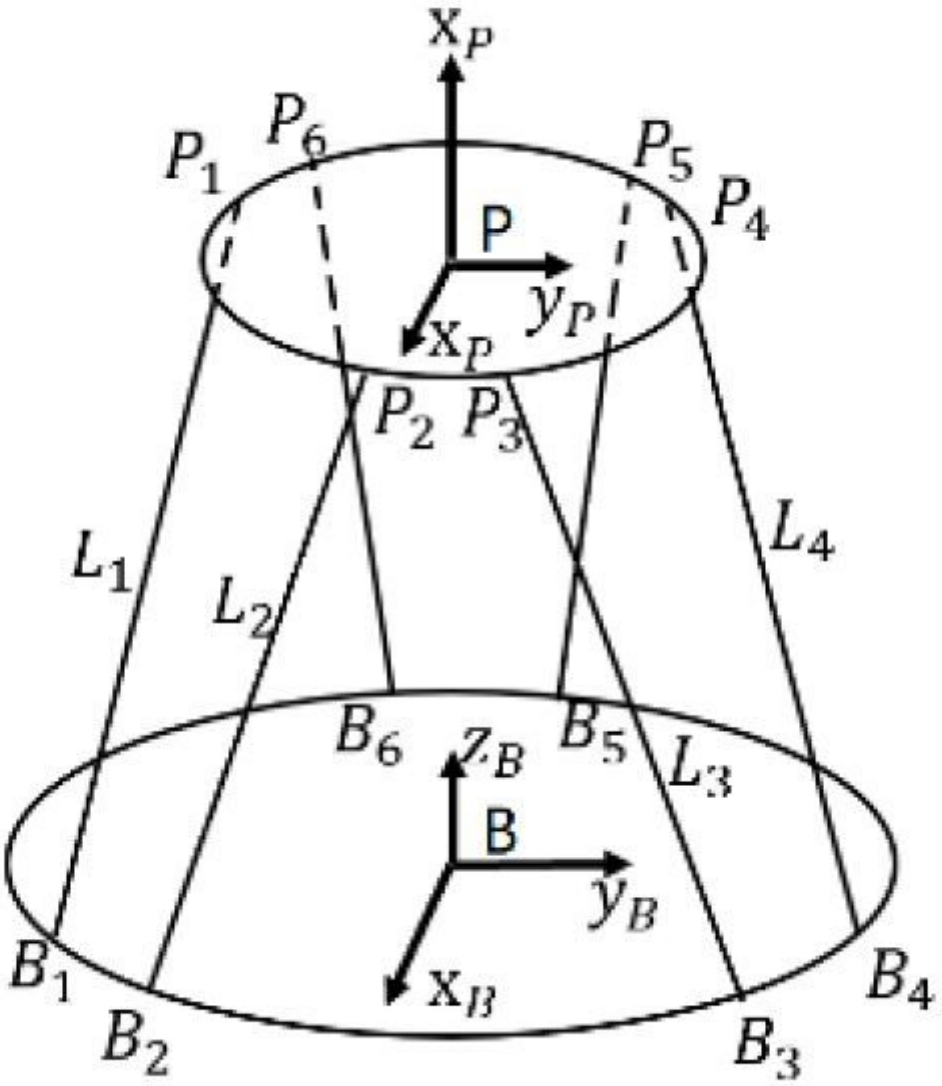

Figure 2

Mecahnical schematic diagram

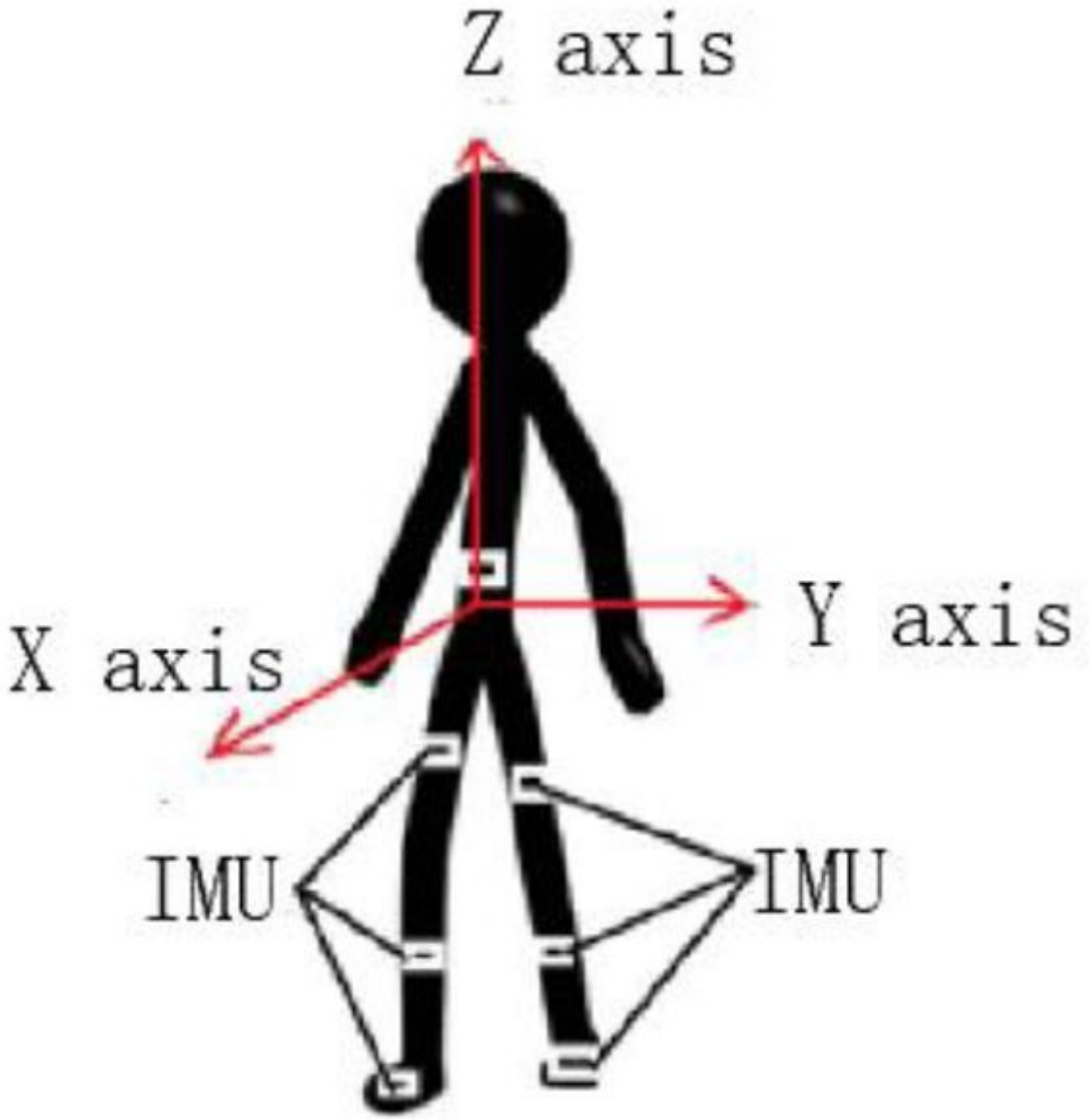

Figure 3

Position of the bounded sensors

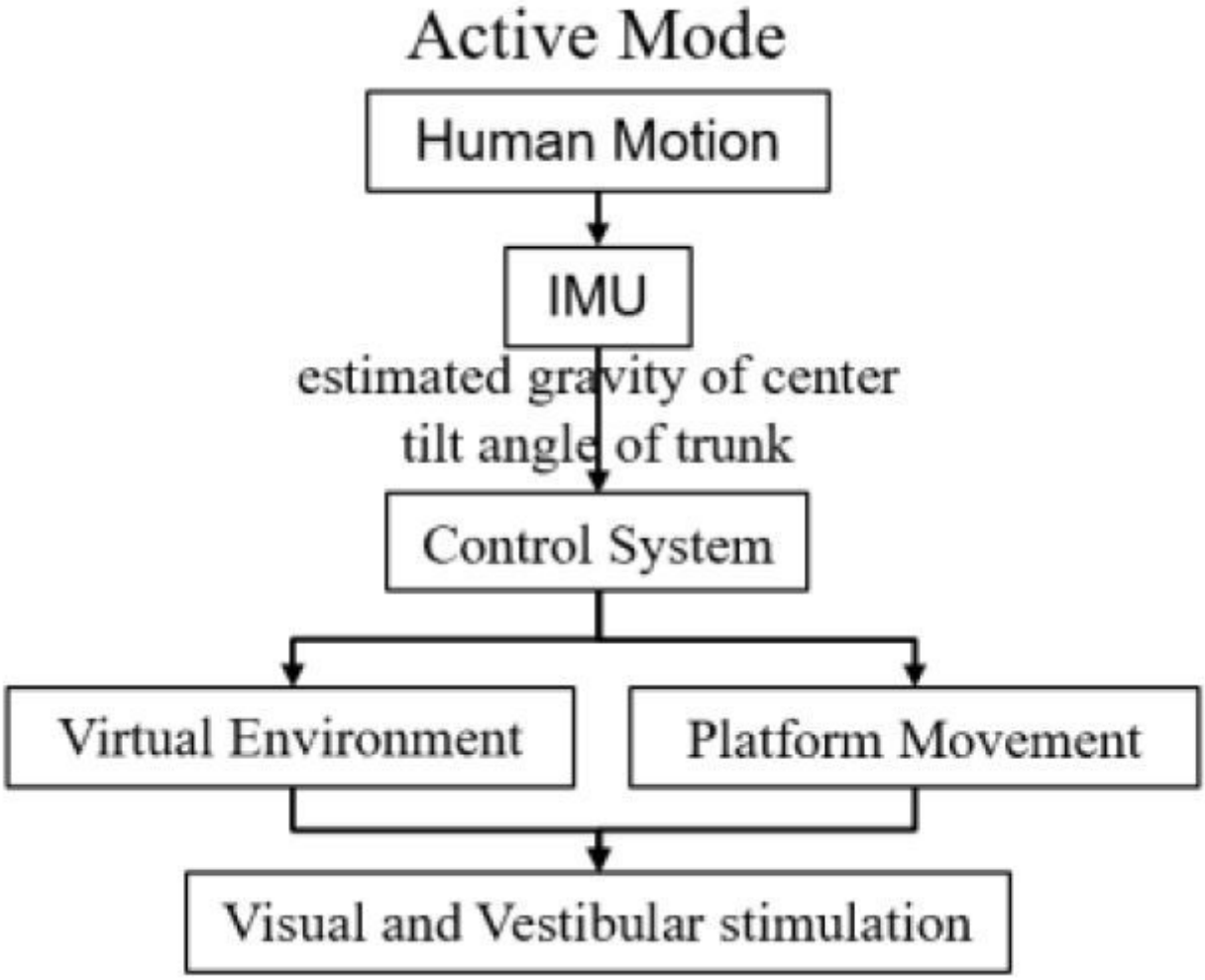

Figure 4

Flow of control signals in active mode

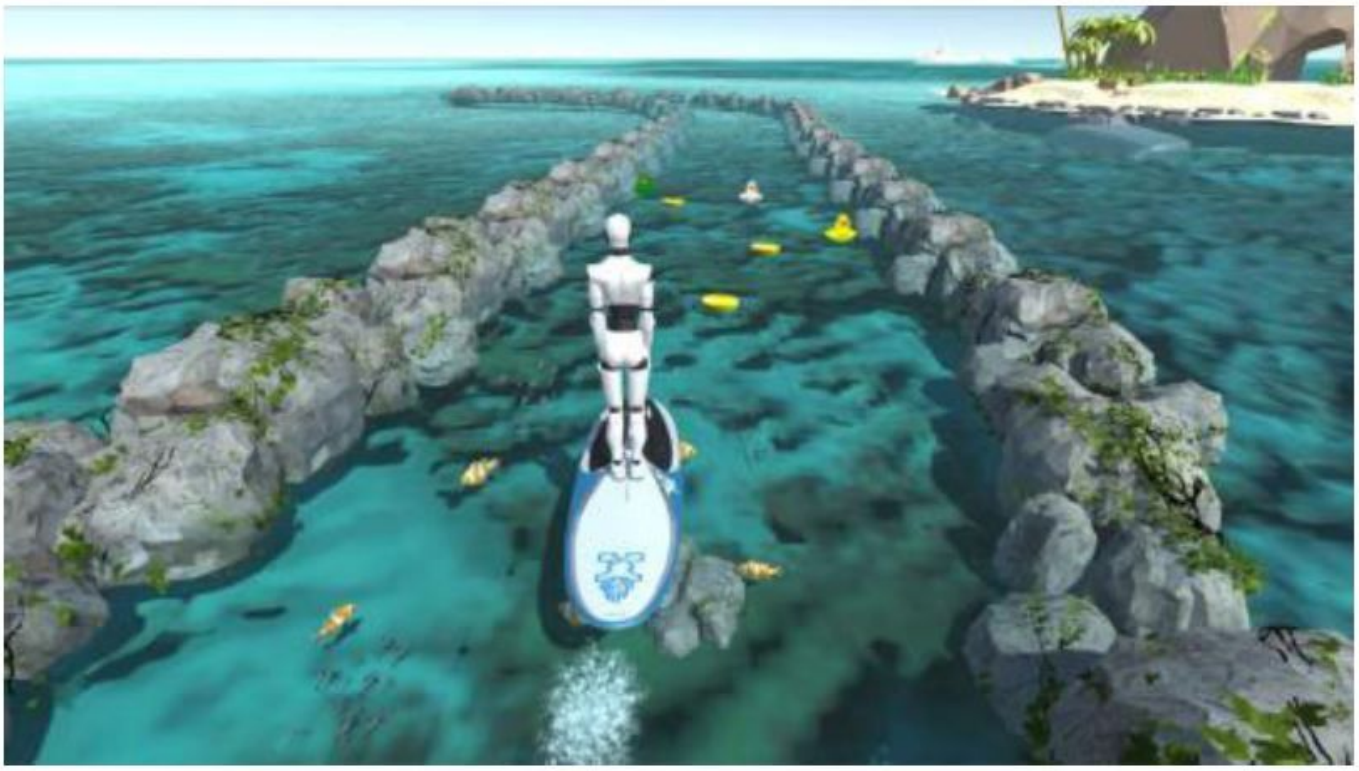

Figure 5

Virtual training scene

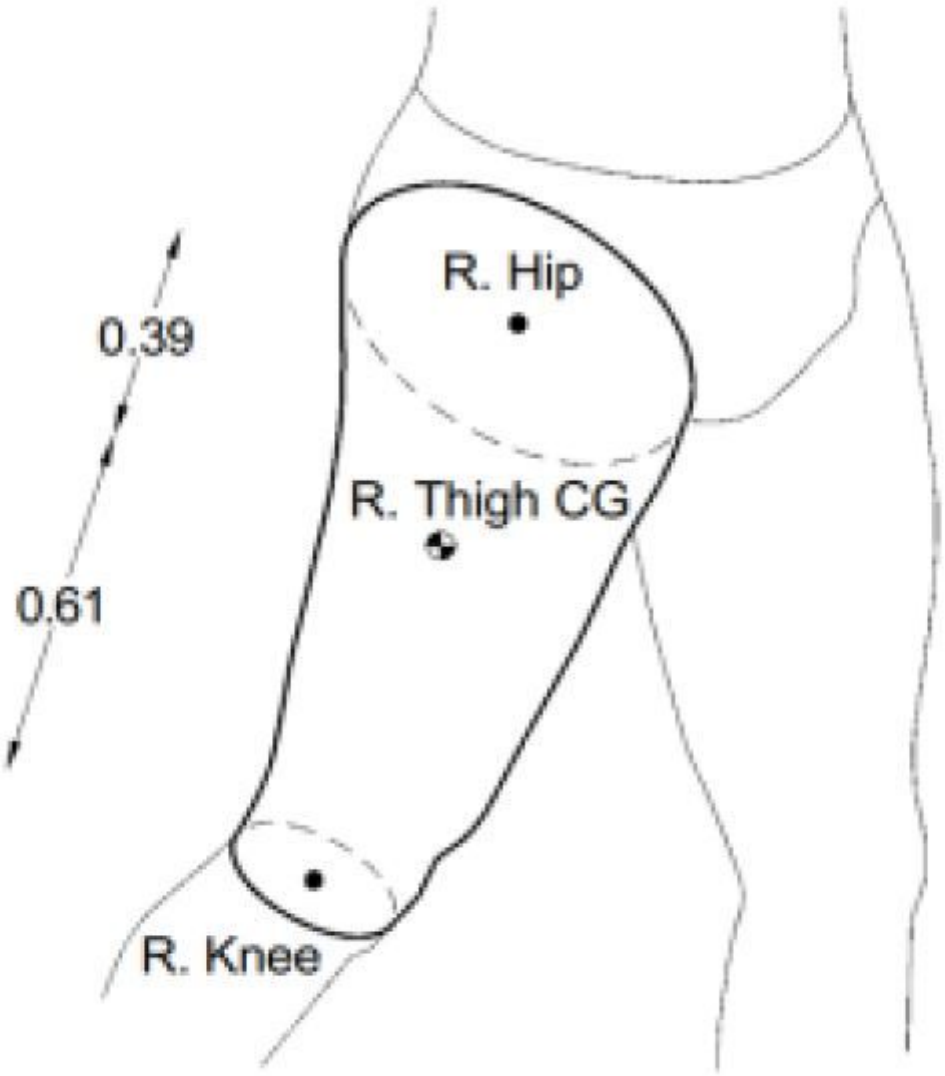

Figure 6

Location of the center of gravity corresponding to adjacent joints

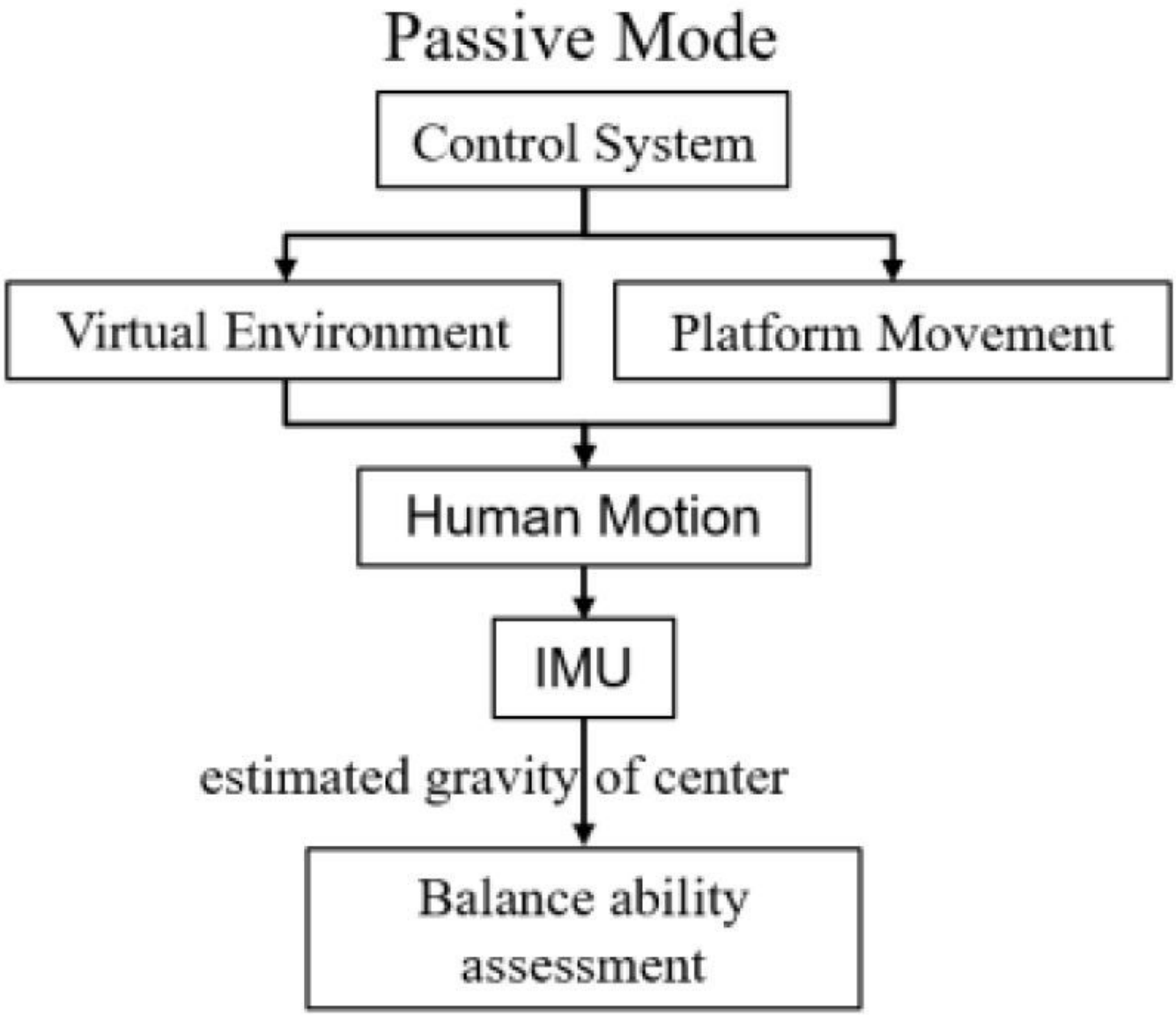

Figure 7

Flow of signals in passive mode

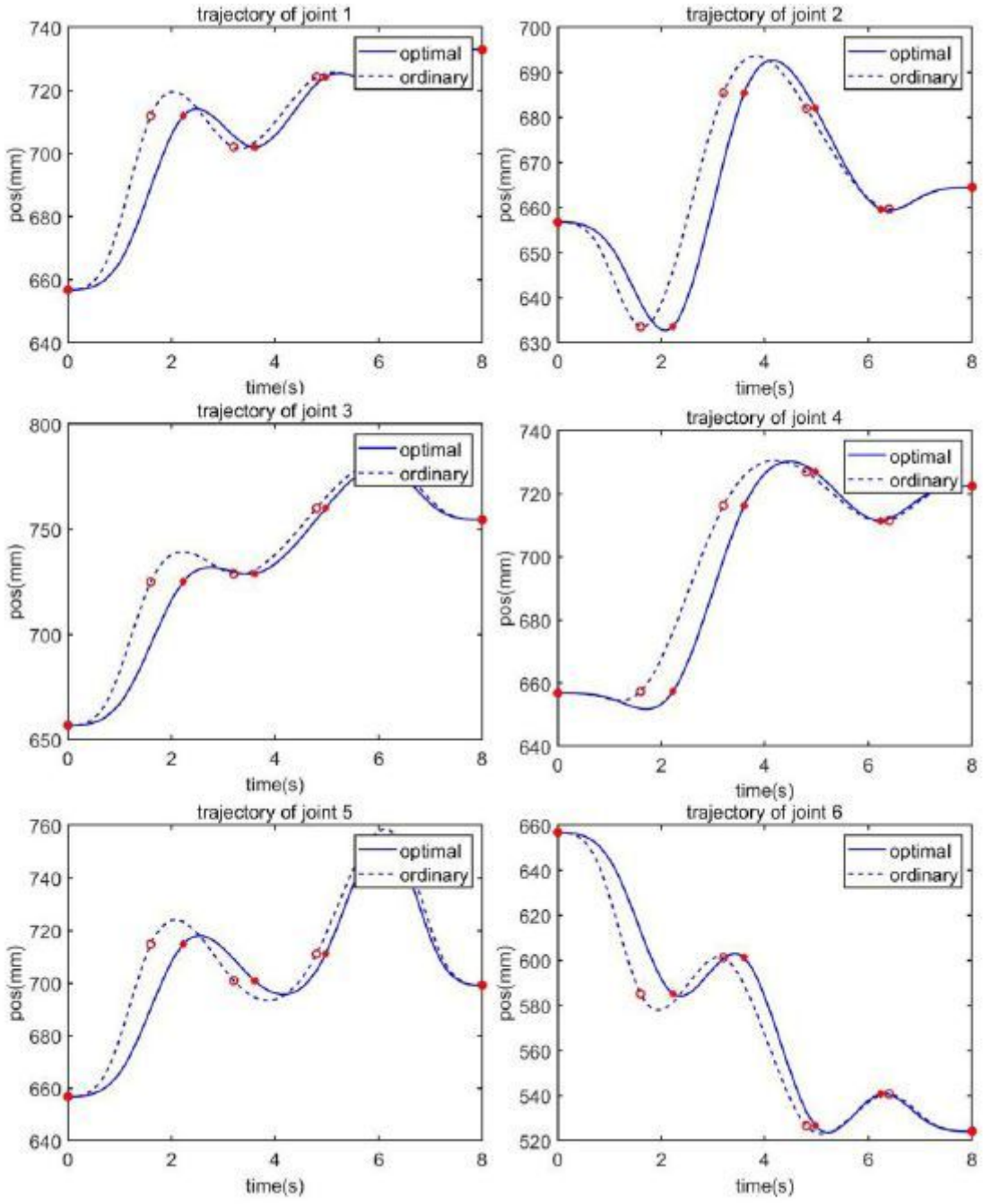

Figure 8

Trajectory of joints

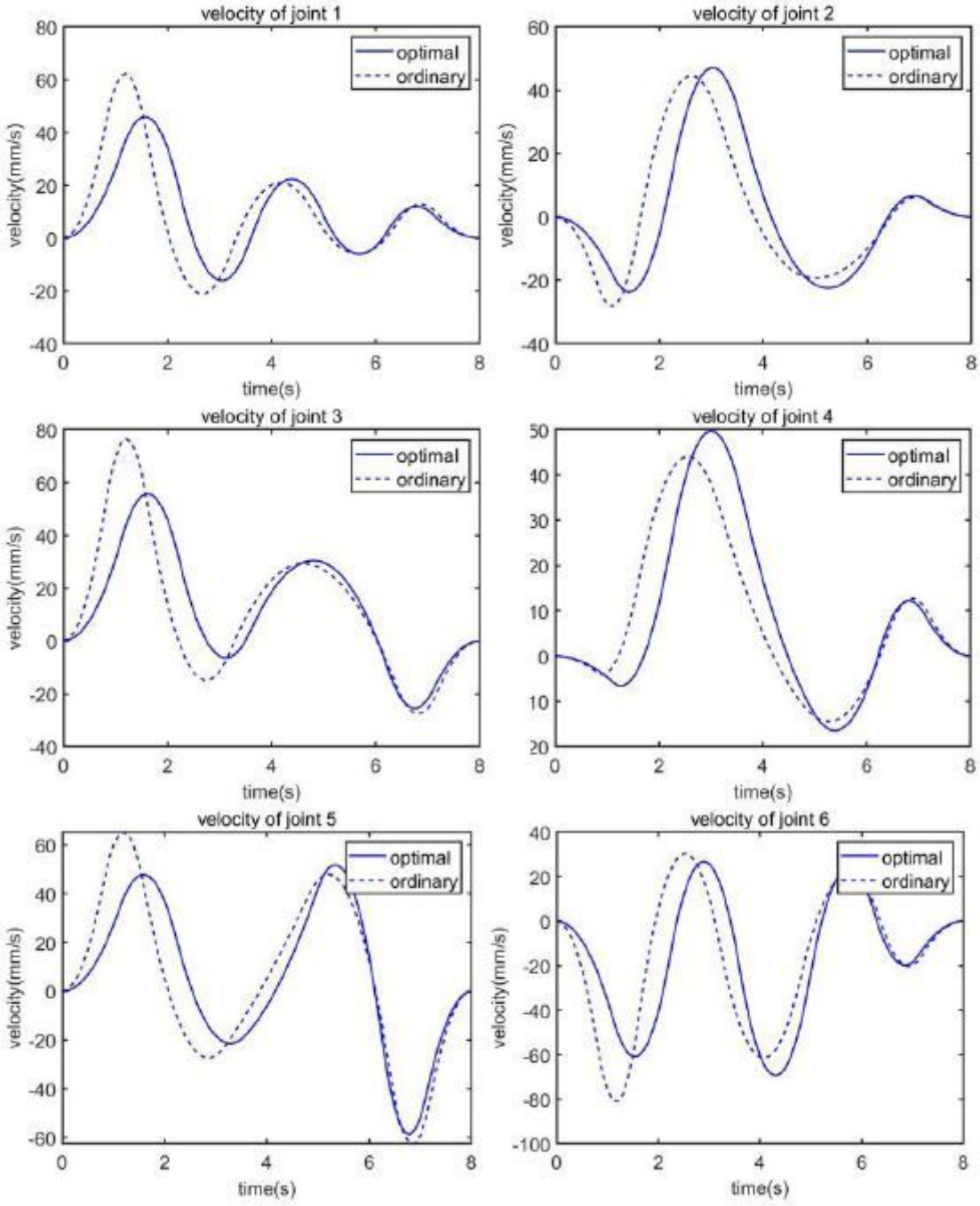

Figure 9

Velocity of joints

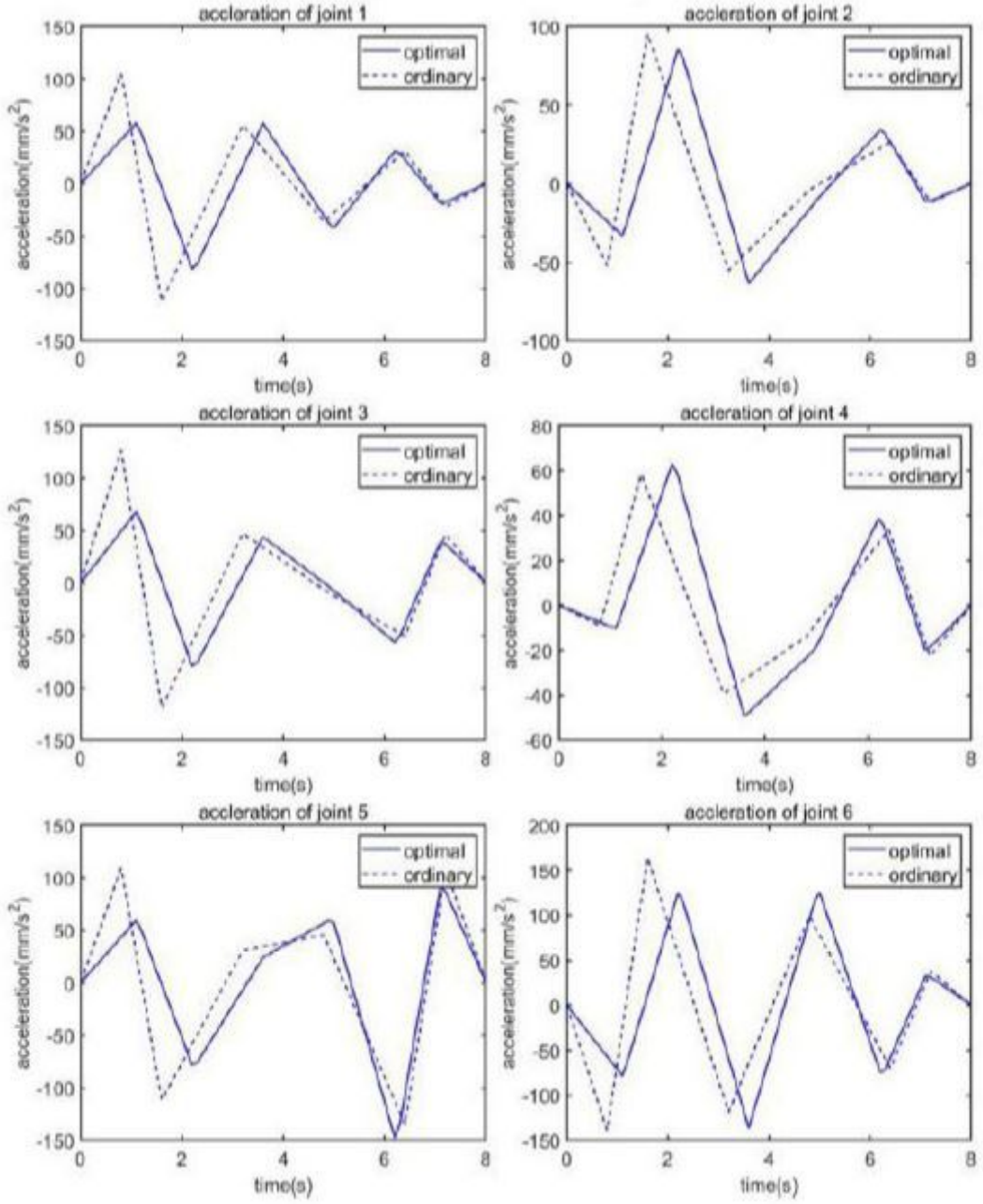

Figure 10

Acceleration of joints

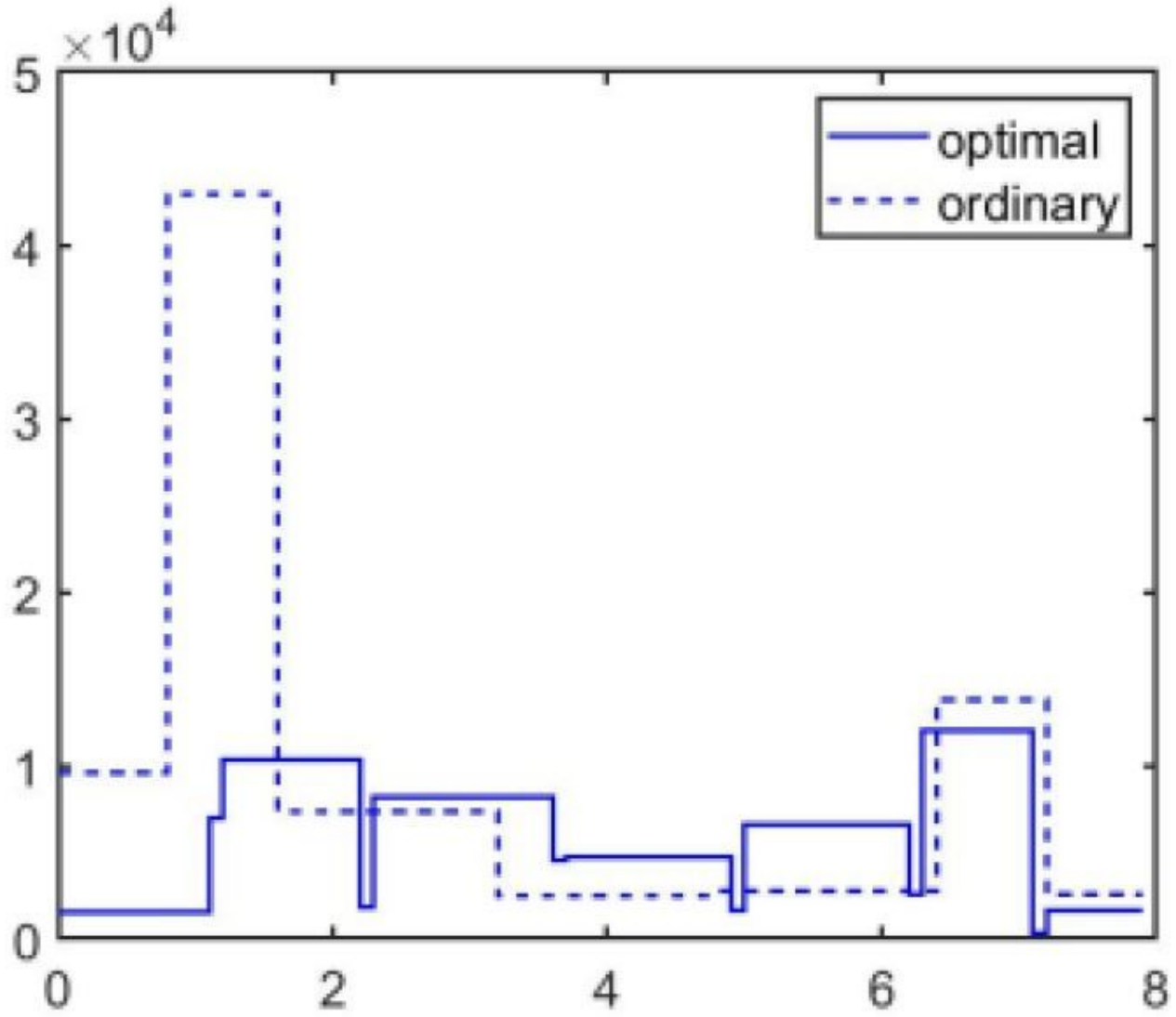

Figure 11

Jerk of joints